# Transneptunian Orbit Computation

**Jenni Virtanen**
*Finnish Geodetic Institute*

**Gonzalo Tancredi**
*University of Uruguay*

**G. M. Bernstein**
*University of Pennsylvania*

**Timothy Spahr**
*Smithsonian Astrophysical Observatory*

**Karri Muinonen**
*University of Helsinki*

We review the orbit computation problem for the transneptunian population. For these distant objects, the problem is characterized by their short observed orbital arcs, which are known to be coupled with large uncertainties in orbital elements. Currently, the observations of even the best observed objects, such as the first-ever transneptunian object (TNO), Pluto, cover only a fraction of their revolution. Furthermore, of the some 1200 objects discovered since 1992, roughly half have observations from only one opposition. To ensure realistic analyses of the population, e.g., in the derivation of unbiased orbital distributions or correlations between orbital and physical properties, realistic estimation of orbital uncertainties is important. We describe the inverse problem of orbit computation, emphasizing the short-arc problem and its statistical treatment. The complete solution to the problem can be given in terms of the orbital-element probability density function (p.d.f.), which then serves as a starting point for any further analysis, where knowledge of orbital uncertainties is required. We give an overview of the variety of computational techniques developed for TNO orbital uncertainty estimation in the recent years. After presenting the current orbital distribution, we demonstrate their application to several prediction problems, such as classification, ephemeris prediction, and dynamical analysis of objects. We conclude with some future prospects for TNO orbit computation concerning the forthcoming next-generation surveys, including the anticipated evolution of TNO orbital uncertainties over the coming decades.

## 1. INTRODUCTION

After over a decade of dedicated observations, the transneptunian population of small bodies has recently passed the landmark of 1000 known objects. The observational data for individual objects extend over several decades, but as a population the transneptunian objects (TNOs) are still characterized by their short observed orbital arcs.

Due to their distance from the observer as well as their long orbital periods, observing the population can be both costly and tedious. Both discovery and followup observations have mostly been acquired in dedicated surveys that have been adapted to the slow motions and faint magnitudes of the targets. While many of the first discoveries were made in the pencil-beam surveys (e.g., *Gladman et al.,* 1998), a large portion of observing efforts have subsequently been carried out by the Deep Ecliptic Survey (*Millis et al.,* 2002; *Elliot et al.,* 2005). While the number of well-observed objects has been steadily increasing, so has the number of unfollowed discoveries: In the 2000s, roughly half the TNOs discovered each year have remained as one-apparition objects, which is also the fraction of one-apparition objects in the current population (as of May 2006). It is worth noting that one of the earliest TNO discoveries, 1993 RP, remains lost some 13 years after discovery.

In the chain of efforts to analyze the observed population, orbit computation is in practice the first task to be accomplished. It is also a critical one, since all followup

questions depend, in one way or the other, on the orbital elements, which need to be derived already from the often-limited discovery data. For the individual objects, ephemeris predictions for followup observations require reasonable estimates for the orbital elements as well as their uncertainties. For the population, realistic evaluation of uncertainties from astrometric data offer the starting point for the derivation of unbiased orbital distributions (see the chapter by Kavelaars et al.) and for analyzing the dynamical structure of the transneptunian region (chapter by Gladman et al., hereafter G07).

The short-arc orbit computation problem has been extensively studied for the inner solar system, particularly in the recent years in the quest for Earth-approaching asteroids. A great number of numerical techniques have been developed to derive orbits for asteroids since the discovery of asteroid Ceres in 1801. We refer to *Bowell et al.* (2002) and *Milani et al.* (2002) for general reviews of the progress made in the past decade and restrict ourselves to those advances particularly relevant for TNOs. The most important development has been the change in viewpoint from determination of orbits to estimation of orbital uncertainty. Many of the advances are related to nonlinear uncertainty estimation, which is essential for short arcs, or to specific use of the linear approximation, particularly for TNOs.

This active research has resulted in new tools for the users of the end product, the orbital elements, either by means of software or orbital databases, both of which we describe in the current chapter. The orbits of TNOs are nowadays made available, in essence, through four well-established web-based services: at the Minor Planet Center (MPC), at Lowell Observatory, at the University of Pisa ("AstDys"), and at the Jet Propulsion Laboratory (JPL). The MPC maintains a database of TNO orbits together with all their astrometric data. Careful checking of incoming observations and putative identifications by MPC staff limits the number of incorrect observations or identifications for these objects, and as a result the MPC database is probably >99% accurate in terms of matching the proper observations and orbits. It is worth noting that with such sparsely observed objects, bad linkages can occur at fairly high rates, and these linkages can often result in an acceptable differential correction but also a spurious orbit. Of the four services, the AstDys and JPL databases provide also formal orbital uncertainties for the objects in terms of covariance matrices. In addition, AstDys also offers proper elements for outer-solar-system objects. Ephemeris prediction service TNOEPH (*Granvik et al.,* 2003) is on the other hand the first web-based realization of nonlinear uncertainty propagation.

The chapter is organized as follows. We first describe the inverse problem of orbit computation, emphasizing the short-arc problem and its statistical treatment. We demonstrate the use of various computational techniques developed for TNOs (section 2) and evaluate the current orbital uncertainties for the observed population (section 3). In section 4, we discuss the orbital distributions in connection with several prediction problems, such as classification and ephemeris prediction. In section 5, we conclude with some future prospects for TNO orbit computation.

## 2. ORBITAL INVERSION AND UNCERTAINTY ESTIMATION

In orbital inversion, we want to derive information on the orbital parameters from astrometric observations. Through the awareness of the existing uncertainty in observed asteroid positions, orbits are today treated in a probabilistic fashion. A fundamental question in orbital inversion is the accuracy of the parameters derived. The orbital elements are often not used as such, rather one wants to have an estimate for their *uncertainty* that can then be propagated to another epoch in time or to different parameter space (e.g., to sky-plane coordinates). According to statistical inverse theory (e.g., *Lehtinen,* 1988; *Menke,* 1989), the complete solution to the inversion is given in terms of an orbital-element probability density function (p.d.f.). While the evaluation of the p.d.f. can be a complicated task, the advantage is that, once derived, there is no need for additional error analysis, which is sometimes a major obstacle in traditional, deterministic approaches. Access to the full p.d.f. is useful, if not crucial, in many applications. This is the case when evaluating collision probabilities, which rely on knowledge of the orbital-element p.d.f., or when analyzing the orbital characteristics of small bodies as a population, as in the present paper.

### 2.1. Statistical Inverse Problem

In the following, we will summarize the formulation of orbit computation in the framework of statistical inverse theory following *Muinonen and Bowell* (1993). The principal idea is that all the available information involved in the inversion can be presented with the *a posteriori* probability density for the orbital elements.

There are several choices for the parameterization of orbits; we denote the osculating orbital elements of an asteroid at a given epoch $t_0$ by the six-vector $\mathbf{P}$. The Cartesian elements $\mathbf{P} = (X, Y, Z, \dot{X}, \dot{Y}, \dot{Z})^T$ are well-suited for numerical computations; in a given Cartesian reference frame, the coordinates $(X, Y, Z)^T$ denote the position and the coordinates $(\dot{X}, \dot{Y}, \dot{Z})^T$ the velocity (T is transpose). For illustrative purposes, we use Keplerian elements, $\mathbf{P} = (a, e, i, \Omega, \omega, M_0)^T$ and the elements are, respectively, the semimajor axis, eccentricity, inclination, longitude of ascending node, argument of perihelion, and mean anomaly. The three angular elements i, $\Omega$, and $\omega$ are currently referred to the ecliptic at equinox J2000.0. The equations describing the inverse problem are the *observation equations*

$$\psi = \Psi(\mathbf{P},\mathbf{t}) + \varepsilon \qquad (1)$$

which relate the astrometric observations $\psi = (\alpha_1, \delta_1; \ldots;$

$\alpha_N, \delta_N)^T$ made at times $\mathbf{t} = (t_1, \ldots, t_N)^T$ to the theory, $\Psi(\mathbf{P}, \mathbf{t})$, and where $\varepsilon = (\varepsilon_1^{(\alpha)}, \varepsilon_1^{(\delta)}; \ldots; \varepsilon_N^{(\alpha)}, \varepsilon_N^{(\delta)})^T$ describe the (random) observational errors.

According to the statistical inverse theory, the solution of these equations is the *a posteriori* probability density, $p_p$, for the orbital elements

$$p_p(\mathbf{P}) \propto p_{pr}(\mathbf{P}) p(\psi|\mathbf{P}) \tag{2}$$

The ingredients needed for its construction are (1) *a priori* probability density $p_{pr}$ for the unknown parameters $\mathbf{P}$; (2) the conditional density of the observations $p(\psi|\mathbf{P})$ expressed with the observational error p.d.f., $p_\varepsilon$. Or in practice, $p_\varepsilon(\Delta\psi)$, as evaluated for the O–C ("observed minus computed") residuals $\Delta\psi$ (see equation (1)).

The equation above is also one form of Bayes' theorem, which enables the user to bring *a priori* information to the inversion process. Despite its controversial nature, the Bayesian approach has in practice turned out to be very useful in many applications. When the solved-for parameters have large uncertainties, *a priori* information can sometimes be used to constrain wide *a posteriori* p.d.f.s. Furthermore, *Muinonen et al.* (2001) pointed out that when solving for $p_p$ in nonlinear inversion, the invariance of the inverse solution under parameter transformations can only be guaranteed by introducing a regularizing *a priori* p.d.f. (e.g., *Mosegaard and Tarantola,* 2002). They suggested the use of Jeffreys's prior (*Jeffreys,* 1946; see also *Box and Tiao,* 1973)

$$p_{pr}(\mathbf{P}) \propto \sqrt{\det\Sigma^{-1}(\mathbf{P})} \tag{3}$$

where $\Sigma$ is the information matrix, or inverse covariance matrix, for the orbital elements. [The information matrix for the orbital elements follows from the inverse covariance matrix for the observations (taken to be known) and the partial derivatives between the parameters and the observed coordinates (computed analytically or numerically).] *Virtanen and Muinonen* (2006) demonstrated that securing the invariance can be crucial when deriving probability measures, such as impact probability, for very short-arc objects. For well-observed objects, the regularizing prior can typically be assumed constant (section 2.2).

The second ingredient in equation (2) is the error p.d.f. Ideally, the observational data should include a complete error model, but this is rarely the case (cf. future surveys such as Gaia). In fact, in the current format of distribution of astrometric observations, no information on measurement errors is included, thus the orbit computer needs to make an educated guess for the distribution of errors. A practical assumption is a multivariate Gaussian noise probability density with zero mean

$$p(\varepsilon;\Lambda) = \frac{1}{(2\pi)^{2N}\sqrt{\det\Lambda}} \exp\left[-\frac{1}{2}\varepsilon^T\Lambda^{-1}\varepsilon\right] \tag{4}$$

where $\Lambda$ is the joint $2N \times 2N$ error covariance matrix of the angular observations. Typically, the observed angular coordinates are taken to be independent, although the above form for the error model allows the inclusion of correlation information when available.

Finally, we can write the *a posteriori* orbital-element probability density as

$$p_p(\mathbf{P}) \propto \sqrt{\det\Sigma^{-1}(\mathbf{P})}\, \exp\left[-\frac{1}{2}\chi^2(\mathbf{P})\right] \tag{5}$$

where $\chi^2 = \Delta\psi^T\Lambda^{-1}\Delta\psi$ is evaluated for the elements $\mathbf{P}$.

The Gaussian assumption, although widely used, has also been shown to fail. Again, in the ideal case, the measurement errors should be more or less randomly distributed. However, the observations can include (unknown, i.e., not corrected) systematic errors, and their distribution can have non-Gaussian features (*Carpino et al.,* 2003). Inversion results can be highly sensitive to the noise assumption (e.g., *Virtanen and Muinonen,* 2006), and thus the handling of observational errors is an important feature of any inversion technique. Transneptunian object astrometry already typically has well-confined measurement errors, at the 0.1-arcsec level. It is expected that astrometric error modeling in general will be improving in the future, due to improving measurement accuracy of the coming surveys (see section 3.1) and improving documentation (the pending new format for astrometric data). However, as the measurement accuracies improve to the milliarcsec level, the modeling demands will also be increasing as the angular difference between photocenter and barycenter will become detectable (*Kaasalainen et al.,* 2005).

How should we characterize the p.d.f.? Numerical techniques for solving the p.d.f. can roughly be divided into two categories: (1) point estimates and (2) p.d.f. sampling via Monte Carlo (MC) means. Point estimates — obtained through optimization methods — are typically sets of parameters describing the p.d.f., such as the least-squares solution, which consists of the maximum likelihood (ML) orbital elements and their covariance matrix (section 2.2).

Point estimates typically work in cases with well-confined p.d.f.s, where the parameter uncertainties are relatively small. For p.d.f.s spreading over a wide range of values in the parameter space, point estimates can be misleading and the only way to reliably characterize the p.d.f. is via MC sampling. While the use of point-estimate methods may be tempting, e.g., due to their speed, many MC methods are today equally feasible thanks to improving computer resources.

Since the observation equations are nonlinear, an important factor when considering the variety of available techniques is their degree of linearity. To highlight the need for the validity consideration, we describe the different methods in two parts: first, techniques relying on the linear approximation and, second, fully nonlinear techniques.

### 2.2. Linearization in Uncertainty Estimation

In the linear approximation, the relationship between the observations and the parameters in equation (1) can be linearized as

$$\Psi(\mathbf{P},t) = \Psi(\mathbf{P}_{ls},t) + \sum_{j=1}^{6} \Delta P_j \frac{\partial \Psi}{\partial P_j}(\mathbf{P}_{ls},t)$$

which is valid in the vicinity of the reference orbit, $\mathbf{P}_{ls}$, denoting the least-squares orbital elements, and where $\Delta\mathbf{P} = \mathbf{P} - \mathbf{P}_{ls}$. Introducing the approximation through equations (1) and (5), the resulting orbital-element p.d.f. is Gaussian

$$p_p(\mathbf{P}) \propto \sqrt{\det\Sigma^{-1}(\mathbf{P}_{ls})} \cdot \exp\left[-\frac{1}{2}\Delta\mathbf{P}^T\Sigma^{-1}(\mathbf{P}_{ls})\Delta\mathbf{P}\right] \quad (6)$$

Here assuming constant *a priori* p.d.f. is acceptable, $\det\Sigma^{-1}(\mathbf{P}) \approx \det\Sigma^{-1}(\mathbf{P}_{ls})$, because the exponential part of equation (6) makes the p.d.f. well-confined. The least-squares orbital elements $\mathbf{P}_{ls}$ are obtained through a differential correction procedure, and the covariance matrix follows from linearized propagation of uncertainties

$$\Sigma(\mathbf{P}_{ls}) = \left(\frac{\partial\mathbf{P}}{\partial\psi}\right)^T_{ls} \Sigma(\psi) \left(\frac{\partial\mathbf{P}}{\partial\psi}\right)_{ls} \quad (7)$$

where $\Sigma(\psi) = \Lambda$. $\mathbf{P}_{ls}$ coincides with the ML estimate, and together with the covariance matrix $\Sigma$, constitutes the full, concise solution to the inverse problem [LSL; nonlinear least-squares with linearized covariances; see, e.g., *Muinonen et al.* (2006) for details].

The covariance matrix defines a six-dimensional uncertainty region in the orbital-element space, centered on the ls orbit

$$\Delta\chi^2 = (\mathbf{P} - \mathbf{P}_{ls})^T\Sigma^{-1}(\mathbf{P}_{ls})(\mathbf{P} - \mathbf{P}_{ls}) \quad (8)$$

For practical purposes, the element uncertainty can be described using the projections of this six-dimensional error hyperellipsoid. By replacing $\psi \rightarrow \mathbf{P}$ and $\mathbf{P} \rightarrow \mathbf{F}$, equation (7) is the general law of error propagation and can be used to transform the orbital uncertainties into new set of parameters, **F**, sky-plane uncertainties, for example.

When describing the method of Bernstein and Khushalani, *Bernstein and Khushalani* (2000, hereafter BK) note that the TNO population presents several simplifications over the general orbit-fitting problem that greatly extend the utility of linearized fitting. For the TNOs, it is possible to choose a basis for the orbital elements such that degeneracies or uncertainties large enough to invalidate the linearization are confined to one of the six elements for arcs of ≈1 week or longer, and are well understood even for single-night arcs.

BK choose a Cartesian coordinate system with z axis along the Earth–TNO vector at the first observation epoch. If we expand the apparent motion in powers of the inverse distance $\gamma \equiv (1\ \mathrm{AU})/z$, then the fact that $\gamma \leq 10^{-1.5}$ for TNOs means that only the first few terms are important, until the orbit becomes very well determined — at which point a linearized solution is accurate for any choice of orbital elements. For example, the transverse gravitational acceleration of the TNO is $\gamma^3$ smaller than that of Earth, and can hence be largely ignored until the orbit solution reaches high accuracy.

The BK orbital element set is $\{x/z, y/z, \dot{x}/z, \dot{y}/z, \gamma = 1/z, \dot{z}/z\}$. The first two elements are simply the angular position at the first observation, hence are well constrained immediately. A second observation determines the angular velocity $\dot{x}/z - \gamma\dot{x}_E$, where the second term is the reflex from Earth's motion. Hence the third, fourth, and fifth elements are degenerately constrained by a pair of observations. This degeneracy is broken by an arc long enough to determine the angular acceleration, which is $\approx\gamma\ddot{x}_E$. From the ground, an arc of ≈1 week suffices to determine γ, except for targets near opposition; from Hubble Space Telescope (HST), a single orbit often suffices to determine distance, as the reflex of the spacecraft orbit gives a detectable parallax.

The last BK element, $\dot{z}/z$, generally requires multiopposition arcs for precise constraint. It is intuitive that the line-of-sight velocity is the most difficult Cartesian element to discern from imaging data. The counterpoint is that ephemerides are quite insensitive to this orbital element (as long as the orbit is bound), and hence a determination of the first five BK elements can provide ephemerides (and uncertainties) that are sufficiently accurate for scheduling recovery observations several years into the future. Thus while a poor constraint on the sixth BK element precludes the determination of Keplerian elements and hence assignment to a TNO dynamical class, the BK system does allow linearized fitting to make full use of the information available in a short arc. Once the arc is long enough to constrain all six elements, then the error ellipse in the six BK elements is straightforwardly transformed into Cartesian or Keplerian elements via equation (7).

*Kristensen* (2004) derives a linearization of the TNO equations of motion that is more accurate than the BK version, yielding arcsecond precision for typical orbits over one-year arcs. Linearizations of some potential prior distributions are also presented by Kristensen. It is hence possible to work with orbit parameterizations that are trivially solved and in which the p.d.f.s are strictly Gaussian, assuming Gaussian errors for the observations.

The nearly inertial motion of TNOs eliminates the multiple branches of short-arc solutions that sometimes arise for asteroids, and the BK fitting process is very fast and robust. This simplicity, plus the ability to produce ephemerides for recovery (with error ellipses), have made the method popular for observers. The BK code becomes less convenient for objects interior to Jupiter's orbit, as the expansion in γ converges poorly. BK is poorly suited to investigations in which the likelihood distribution along poorly constrained elements is important, e.g., attempting to infer the

Keplerian-element distribution for populations of short-arc objects. In such cases a fully nonlinear, MC characterization of the likelihood, including relevant priors, is required.

### 2.3. Nonlinear Sampling of Uncertainty

Linear methods typically work well when the orbital uncertainties are well constrained, i.e., relatively small. This is not the case when we are dealing with objects with small amounts of data, either by number or by their orbital arc covered; such data are known to be coupled with large uncertainties. Problems with linear covariance mapping can also arise from other sources than the data. The uncertainties often need to be propagated to another epoch or different parameter space, and this mapping can be strongly nonlinear.

For TNOs, the most obvious problem is connected with their short arcs. While for inner-solar-system objects nonlinear p.d.f.s are well known to result for new discoveries — corresponding to observed arcs from a few hours up to weeks — due to their long orbital periods, the nonlinearities for TNOs can be dominant much longer, up to several years, that is, over several apparitions. Second, long propagations needed, e.g., in solar-system integrations, which may entail additional nonlinearities in terms of deep close approaches with massive bodies, can cause the failure of the linear approximation.

Luckily, there are several ways to solve these problems. For the uncertainty propagation, one solution is to introduce semilinear approximations (see section 2.4). However, when the element uncertainties/nonlinearities are large, they can in practice only be estimated by sampling the uncertainty region with a discrete map. This also solves the propagation problem since the mapping points can be propagated to the desired epoch, or coordinates, individually and nonlinearily. Below, we describe perhaps the most general approach to nonlinear sampling, by Monte Carlo means; we reserve section 2.4 for other advances in the subject.

The MC techniques are based on random sampling in some selected coordinates to generate large numbers of sample orbits mapping the p.d.f. Orbital elements (**P**) can be sampled directly if the p.d.f. is already well-confined, e.g., Gaussian (*Chodas and Yeomans,* 1996; *Muinonen and Bowell,* 1993), or close to being bell-shaped (see VoV technique below). Sampling in observation space (R.A. and Dec.) is practical if the orbital-element p.d.f. is too extended to allow direct sampling (e.g., in BK). If there are very few observations, including the object's unknown topocentric distance in the sampling parameters ("extended" observation space; R.A., Dec., rho) reduces the minimum number of observations needed in the inversion to two (see Ranging below).

In contrast to the linear case, large uncertainties typically imply strongly non-Gaussian p.d.f.s. Methods based on orbital or observational MC typically make use of the linear approximation, in the form of least-squares fitting, while sampling in the extended observation space is in practice the only way to handle strongly nonlinear cases. Below, we describe two nonlinear techniques, the first of which uses linearization as a intermediate step, but both of which result in fully nonlinear p.d.f. sampling.

*2.3.1. Volume-of-variations (VoV).* *Virtanen et al.* (2003) pointed out that, for TNOs, the linear approximation can break down even for the numbered objects. As a solution, they suggested six-dimensional sampling of the uncertainty region using least-squares covariances (see also *Muinonen and Bowell,* 1993), a generalization of the so-called line-of-variation methods (*Milani,* 1999) (section 2.4). *Muinonen et al.* (2006) devised a new technique that samples a six-dimensional volume in the phase space instead of a one-dimensional curve. In the initialization part of VoV, starting from the global LSL solution, local linear approximations are computed for a reduced number of orbital elements as a function of one or more mapping elements. Currently, the semimajor axis or the Cartesian X-coordinate is chosen as the single mapping parameter, and by correcting for the remaining five orbital elements, a discrete set of points corresponding to the local p.d.f. maxima is computed. In the second part, guided by the local linear approximations, MC sampling is introduced in the six-dimensional phase-space volume for a fully nonlinear treatment.

The degree of nonlinearity can be increased in the initialization part by selecting several mapping parameters (e.g., the longitude of the ascending node in addition to semimajor axis), but the technique may quickly become computationally excessive for more numerous mapping parameters. In this paper, the VoV technique has been systematically applied to a large number of TNOs and, at the same time, the technique was fully automated.

*2.3.2. Statistical orbital ranging (Ranging).* When the orbital uncertainties are large, sampling of the p.d.f. in orbital elements is no longer efficient nor possible. *Virtanen et al.* (2001) and *Muinonen et al.* (2001) established the idea of sampling the orbital-element uncertainty in topocentric spherical coordinates. In Ranging, two observation dates are chosen from the complete observation set and the corresponding topocentric distances (or ranges), as well as the R.A. and Dec. angles, are MC sampled using predefined intervals, which are subject to iteration. The two Cartesian positions lead to an unambiguous set of orbital elements based on well-established techniques in celestial mechanics. The elements then qualify as a sample orbit if the fit to the observation set is acceptable. *Virtanen et al.* (2003) applied the automated Ranging to TNOs, presenting the first systematic analysis of the orbital uncertainties of the then-known population.

### 2.4. Other Advances

Another approach to dealing with the nonlinearities in orbit computation was put forward in *Milani* (1999). They have developed one-dimensional techniques based on the line of variations (LOV), which is aligned with the principle axis of the covariance ellipsoid (cf. equation (8)). To overcome the problems faced with linear propagation, they

have proposed semilinear approximations for mapping and propagating orbital uncertainties starting from the LSL (*Milani and Valsecchi,* 1999). The concept of multiple solutions along the LOV has been used for better mapping the orbital uncertainty in many applications such as identification or impact monitoring (*Milani et al.,* 2002, 2005).

For what they term "very short arcs," *Milani et al.* (2004) have taken a geometric approach to uncertainty estimation. Through least-squares fitting in the observation space (two angles and angular rates), they use a set of virtual asteroids to describe the uncertainty region by triangulation of the unknown range-range-rate plane. This approach is also suitable for making ephemeris predictions for Centaurs (*Milani and Knežević,* 2005) but the need for the estimation of angular rates may become problematic for more distant objects due to their slow relative motions (*Milani et al.,* 2006).

Closely resembling the initialization part of VoV, *Chesley* (2005) introduces a two-dimensional plane-of-variation technique that utilizes the range and range rate as the orbital elements to be systematically varied and uses it to estimate the encounter probability for a short-arc asteroid. However, the four remaining dimensions of the inverse problem are not treated.

Techniques similar to Ranging, based on the variation of topocentric coordinates, have been described by others (see, e.g., *Bowell et al.,* 2002, and references therein), but the one by *Goldader and Alcock* (2003) is specifically tailored for TNOs. The idea therein is identical to Ranging as far as the sampling procedure is considered. However, they do not provide solid probabilistic interpretation of the uncertainty mapping, although the two methods produce similar results for the *extent* of the uncertainty region.

The discovery of several multiple systems in the Kuiper belt has spurred research on dynamics of binary objects. Although the particulars of the physical problem differ from the one discussed in the present paper, and are thus omitted here, there are some links between the two problems that we consider worth discussing. Multiple systems are observationally demanding, and optimal datasets for orbit computation can be difficult to obtain. The shortage of data is even more obvious for distant and faint systems such as TNO binaries. Recently, *Hestroffer et al.* (2005) introduce an MC-based sampling to Thiele-Innes method for evaluating the uncertainties in binary orbits in general. As followup observations for TNO binaries are especially costly, Grundy et al. (in preparation) modify Ranging for binary systems to optimize the scheduling of Hubble Space Telescope (HST) observations. Both methods are well-suited for TNO binaries with very sparse data, and can be used to impose realistic uncertainties for the derivable physical parameters, such as the total mass and density of the objects.

## 3. TRANSNEPTUNIAN OBJECT ORBITAL UNCERTAINTIES

To illustrate our current understanding of the orbital uncertainties for the TNO population, we have carried out TNO orbital inversion systematically for the known objects using the orbit computation software package Orb developed at the University of Helsinki Observatory. The package currently provides tools for full, automated orbital inversion of solar system objects, as well as tools for many prediction problems. Below, we demonstrate the use of the statistical techniques just described, in the order of increasing degree of nonlinearity: (nonlinear) least-squares estimation, VoV technique, and Ranging. As a comparison, uncertainties are also evaluated using the BK method, which has been widely used, e.g., for TNO ephemeris prediction.

Some of the questions we would like to discuss here include determining the optimal application regions for the different methods. In particular, as the amount of observational data increases, when do point estimates (vs. sample orbits) become useful? Reflecting the expected improvement in astrometric accuracies, what is the role of observational accuracy in TNO orbital inversion?

We have included in the analysis all outer-solar-system objects listed as transneptunian objects, scattered-disk objects, or Centaurs in the MPC database. As of May 2006, there were 1159 objects, of which 148 were numbered. [In addition, Pluto, numbered (134340) in August 2006, was included for completeness.] For the unnumbered objects, TNO orbital-element p.d.f.s are represented with 2000 sample orbits, which all satisfy the observations with predefined accuracy (requiring both the weight in equation (5) and the O–C residuals to be acceptable). On a modern workstation, the computations for each object took on average two minutes, the typical number of trial orbits needed being some tens of thousands. For numbered objects, least-squares orbital elements and covariance matrices are used. For the observational error p.d.f. in equation (4), we assume uncorrelated R.A. and Dec. p.d.f.s with zero mean and standard deviation of 0.5 arcsec. There was need to adjust this noise assumption for several objects, as discussed below in section 3.1. No Bayesian *a priori* information is imposed in the computations except for the shortest arcs, for which a practical constraint in semimajor axis is used; the maximum allowed value for a was 1000 AU (see *Virtanen and Muinonen,* 2006). Computations were mostly carried out using the two-body dynamical model, but the planetary perturbations were included for the numbered objects. The validity of the two-body approximation was also discussed.

To quantify the results of the orbital inversion, the orbital uncertainties are illustrated in Fig. 1 using two quality metrics (*Muinonen and Bowell,* 1993): the standard deviations ($\sigma$) of the semimajor axis and inclination p.d.f.s. Based on these metrics, as proposed in *Virtanen et al.* (2003), the population can be divided into three categories: one-apparition objects (513), two-apparition objects (96), and multiapparition objects (550). The first category consists of objects that have been observed up to six months and is characterized by very large uncertainties. Semimajor axis, together with eccentricity, is typically poorly determined for short arcs ($\sigma_a >\sim 10$ AU), while inclination can on occasion be determined rather well ($\sigma_i \sim 0.001°$) even with such limited data. The two-apparition objects have been observed in the subsequent opposition after discov-

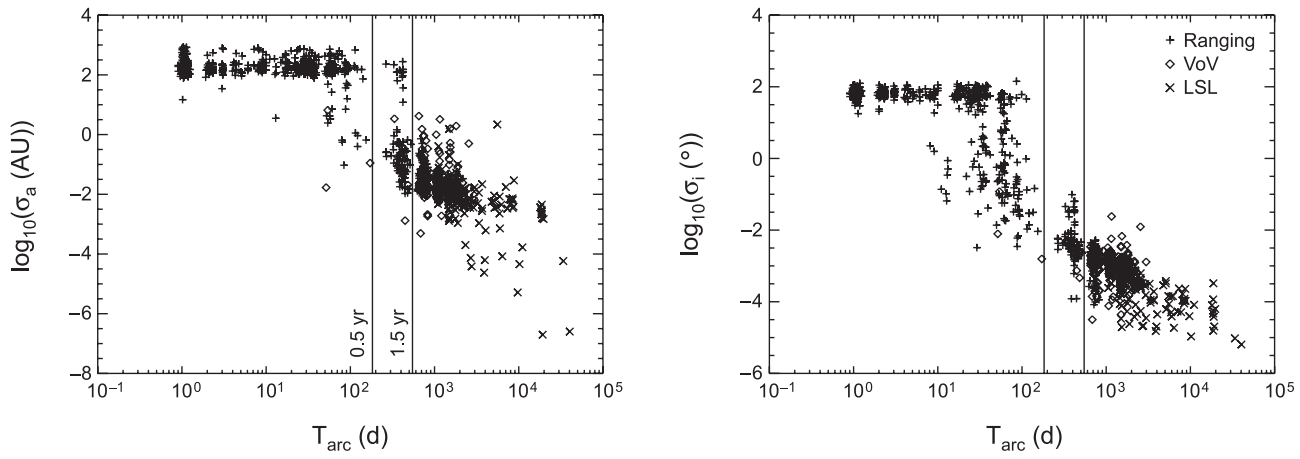


**Fig. 1.** Phase transition in the orbital uncertainties as a function of the length of the observed time arc. Based on the semimajor-axis (left) and inclination (right) standard deviations, objects can be divided into three categories: one-, two-, and multi-apparition. The application of different inverse techniques is also illustrated; Ranging (pluses), VoV (diamonds), LSL (crosses).

ery ($180 < T_{arc} < 540$ d). The accuracy of the orbit varies greatly, and the data can fix the orbital elements rather well, or leave some of the elements very poorly constrained. Multiapparition objects include all the objects with observational arcs longer than 1.5 yr that already have well-confined uncertainties for all the elements.

Figure 2 shows the distribution of TNO orbits using the joint orbital-element p.d.f.s obtained by summing the p.d.f.s for the individual objects, which have been normalized (all objects have equal weights). The histograms for only objects observed on several oppositions (solid curves) display the known characteristics of the region; for semimajor axis, the two largest groupings of objects are the classical belt and the 3:2 resonance population. The inclination p.d.f. shows the twofold structure with low-inclination (<5°, "cold") and high-inclination (10°–30°, "hot") populations. However, the short-arc objects (included in dashed curves) introduce several biases in the joint distributions, which do not show up for longer arcs. Most notably there is an abundance of high-eccentricity orbits that corresponds to the peak at small values for the perihelion distance (q). An *a priori* constraint from the well-observed orbits can be used to smooth away this behavior for short-arc objects.

Since the TNO population includes many very-short-arc objects with small numbers of observations, the applicability of the statistical interpretation of the orbit computation results should be discussed, as pointed out by *Bowell et al.* (2002). The effect of Jeffreys' regularizing *a priori* p.d.f. used to maintain the invariance was monitored for the shortest arcs ($T_{arc} < 180$ d), as suggested by *Virtanen and Muinonen* (2006). The joint p.d.f.s of orbital elements were found to be insensitive to the choice of the prior (Jeffreys' or constant prior). Furthermore, we point out that, when the analysis is based on only a few data points, the orbital element p.d.f. itself may lose its meaning but the extent of the orbital uncertainty can still be mapped. One of the objects analyzed, 2004 $PR_{107}$, had only two observations, on distinct nights. In such a case, the orbital-element p.d.f. can be assumed uniform, i.e., in Ranging, the sample orbits are accepted simply if they produce acceptable residuals at the observation dates.

### 3.1. Phase Transitions

As the orbital uncertainties gradually decrease with increasing observational data, there typically exists a time interval over which the accuracy of the orbit quickly improves. This nonlinear collapse in the uncertainties has been termed the "phase transition" (e.g., *Muinonen and Virtanen,* 2002) and can also be seen in Fig. 1 for the TNO uncertainties. The exact location of the phase transition has been shown to vary from object to object (*Muinonen et al.,* 2006) — depending on the observational data and dynamical class of the object — and it is also different for the different elements. For Keplerian elements, this typically happens first for the inclination and last for semimajor axis and eccentricity. For Cartesian elements, phase transition occurs when the observational data begin to constrain elements to a region that is entirely contained by our expectation of a bound orbit or other prior constraints. The line-of-sight velocity is the orbital element, which takes the longest to be meaningfully constrained by the data.

Figure 1 presents an average or "statistical" view of the phase transition for the whole population. The transition regime coincides with the two-apparition category of objects, among which the scatter in the semimajor-axis uncertainty is the largest. Note that the smallest uncertainties across the time axis typically correspond to the closest Centaur orbits, while the isolated object close to [5000 d, 1 AU] (cross symbol) is (90377) Sedna, one of the most distant TNOs ($a_{ML} = 529$ AU).

The phase transition can help to study when the different techniques described in the previous section can and should be applied. *Virtanen et al.* (2003) already showed that the

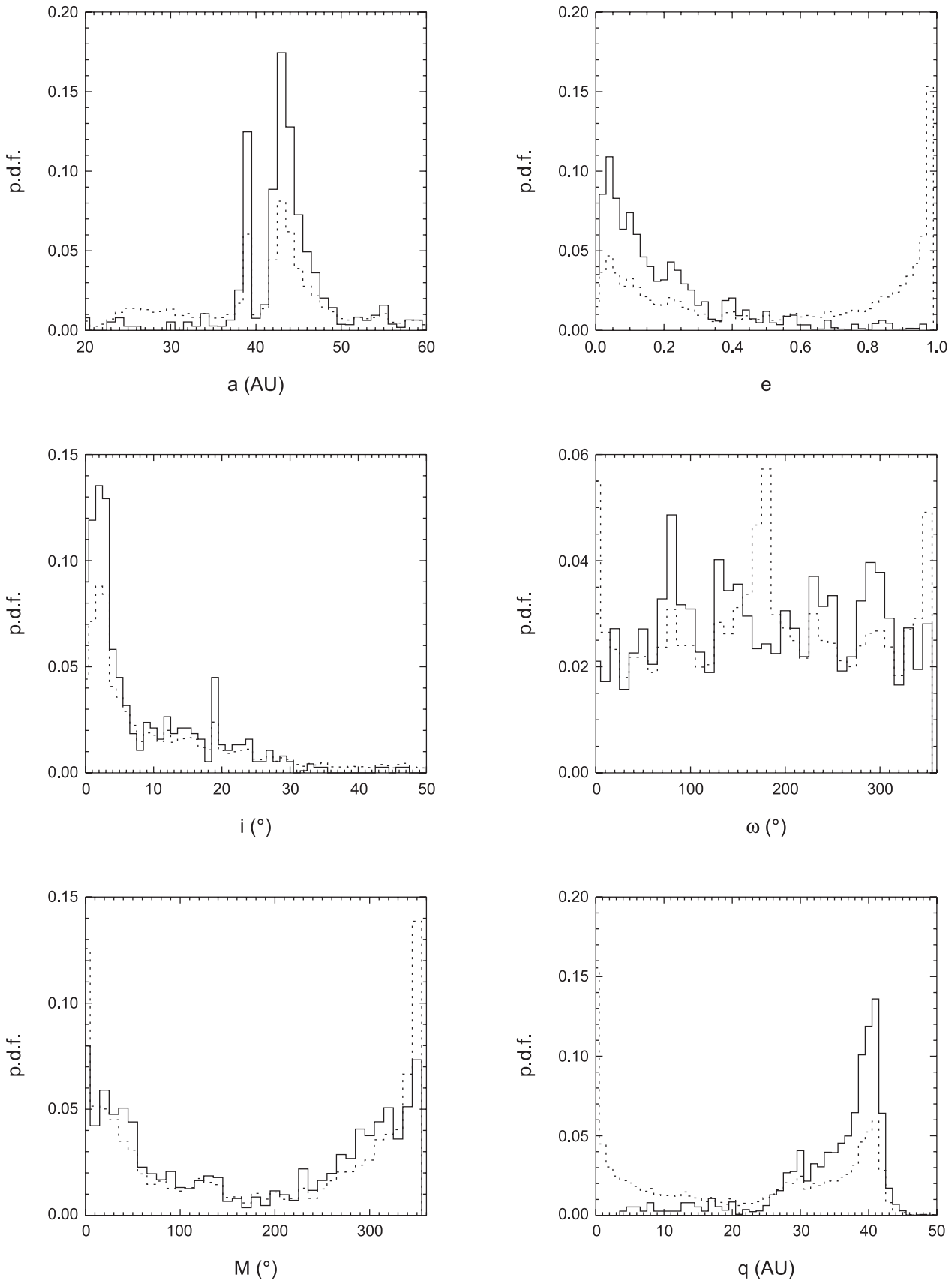


**Fig. 2.** Joint orbital-element p.d.f.s for all known objects (dashed line) and for objects observed longer than $T_{arc} > 180$ d (solid line). The prominent characteristics of the region are clearly visible, but the short-arc objects introduce several biases in the joint distributions, which do not show up for longer arcs.

Ranging technique could be applied to 90% of the population known in 2001, including multiapparition TNOs. Since the fraction of one-apparition objects has been steady at 50%, it was *a priori* clear that most of the computations for unnumbered objects can be carried out using one method. Figure 1 shows Ranging solutions for 736 objects, longest arc extending up to six years of observations (2218 d), which is well beyond the transition regime.

However, the observational data for the known objects has also been steadily growing — numbered objects from 19 (February 2001) to 148 (May 2006), multiapparition objects from 93 to 550 — highlighting the need for efficient methods for longer arcs. Methods such as BK and VoV have been developed for this purpose. The BK method has been put to practice in followup work (see section 4.1). Here we have tested VoV extensively for multiapparition TNOs (272 objects in Fig. 1).

To continue the comparison of the different techniques, we plot the semimajor-axis standard deviations computed using all four methods for a selection of objects (Fig. 3). The uncertainty estimates mostly agree, indicating that the choice of method is not very crucial in estimating modest to small uncertainties. The most notable discrepancies appear when the uncertainties are large, but there are several cases of modest uncertainties where almost order-of-magnitude differences can occur. A defect of the present comparison is that it does not tell about the nonlinear correlations between the elements that may exist and can only be mapped with nonlinear techniques.

As discussed in section 2.1, modeling of observational errors is a significant factor in the orbital inversion process. Once the phase transition occurs, the uncertainties in the orbital elements will scale linearly with the uncertainties in the astrometric data. More precise astrometric data can also

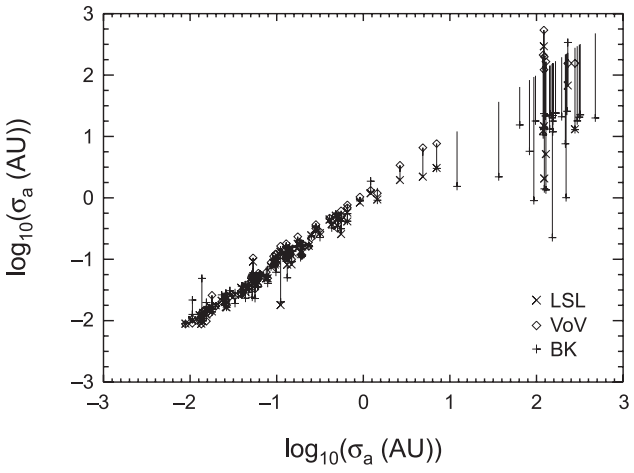


**Fig. 3.** Comparison between orbital uncertainties evaluated using different inversion techniques. Standard deviations of semimajor axis from Ranging in the x-axis and from the other techniques in the y-axis. Note that the largest VoV uncertainties (upper right corner) result from incomplete p.d.f. sampling (constrained by unphysical solutions).

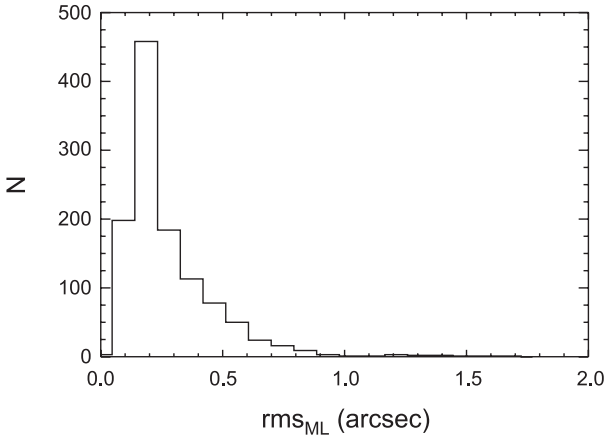


**Fig. 4.** Distribution of the rms values for the maximum likelihood (ML) orbits. For most of the objects, observational data is accurate to ~0.2 arcsec, but there are 14 objects with $rms_{ML}$ > 1.0 arcsec.

shorten the observed time arc required to reach the transition. Since, however, the measurement uncertainty in line-of-sight velocity typically shrinks faster than linearly with arc length, the time of phase transition advances more slowly than linearly with improved astrometric errors.

The current accuracy of TNO astrometry can be estimated from the distribution of O–C residuals. Figure 4 shows the distribution of rms values for the ML orbits. For majority of TNOs, the noise assumption of 0.5 arcsec turned out to be a conservative one; the rms distribution suggests that most of the observational data is accurate to ~0.2 arcsec. However, it is evident that the quality of data varies a lot, as the best-fitting orbits can have rms values from 0.1 to close to 2.0 arcsec. For some 50 multiapparition objects, the large fractions of apparent outliers in their datasets were only reduced by including the planetary perturbations, indicating the failure of two-body approximation. We note that including the perturbations will also reduce the residuals for some objects with large rms. Furthermore, for some 20 objects, acceptable orbit solution could only be found if the assumed R.A. and Dec. standard deviations were increased to 1.0 arcsec. This set of objects included five objects that are TNO binary candidates (see the chapter by Noll et al.). In fact, as the binary systems are rather numerous among known TNOs, residual distributions could be studied to find signatures for unknown binary systems among the known objects.

In astrometry, there are two sources of errors. First is the uncertainty in determination of the TNO position relative to astrometric field stars in its vicinity. Modern groundbased techniques and good PSF fitting, including accurate timing, should reduce this well below 0.1 arcsec, to 10-milliarcsec level for high-S/N objects, and even below for spacebased observations. The second source of ephemeris errors is inaccuracy in the placement of the astrometric standard stars on the global inertial coordinate system. The quality of global astrometric standard systems is improving rapidly,

with the ~0.2-arcsec errors of the USNO-B catalog to be reduced substantially in the next decade by several astrometric surveys (e.g., *Zacharias,* 2004). These include, in the expected "first-light" order, the USNO CCD Astrograph Catalog (UCAC), Panoramic Survey Telescope and Rapid Response System (Pan-STARRS), ESA's Gaia mission, and Large Synoptic Survey Telescope (LSST).

While ESA's astrometric space observatory Gaia can only observe a handful of the brightest TNOs due to its limiting magnitude of ~20 (F. Mignard, personal communication), it will do so with accuracies in the 10-microarcsec level at best. On the other hand, Pan-STARRS is expected to discover large numbers of objects, but with a more modest accuracy of some 10 milliarcsec (*Jedicke et al.,* 2007). To study the influence of the improving accuracy on orbital uncertainties, we created simulated sets of observations for an object on a distant orbit by assuming different astrometric accuracies. The orbit and observing dates correspond to TNO (87269), which has a semimajor axis of 550 AU and eccentricity of 0.96. The original dataset was broken down night by night, and the observations were simulated with accuracies of 0.5, 0.005, and 0.00005 arcsec. Figure 5 shows the phase transition in the observational accuracy. For the longer arc lengths, there is a linear trend: an order-of-magnitude improvement in the observational accuracy results in a similar improvement in the orbital accuracy. On the other hand, to reach a given orbital accuracy, an improvement of 2 orders of magnitude in the astrometric accuracy implies a decrease of 1 order in the length of observational arc required.

### 3.2. Filtering Unstable Orbits

Up to now we have not made any specific considerations about the dynamical properties of the orbit solutions computed. The transneptunian region is supposed to be a reservoir of objects that has lasted since the origin of the solar system, with objects henceforth slowly leaking away or entering into planet-crossing orbits (e.g., the Centaurs). The lifetime during the planet-crossing state is several orders of magnitudes shorter than the time spent in the transneptunian region. Therefore, it could be expected that most of the objects were in stable nonencountering orbits, and only a small proportion of objects might have unstable orbits allowing encounters with the planets at present.

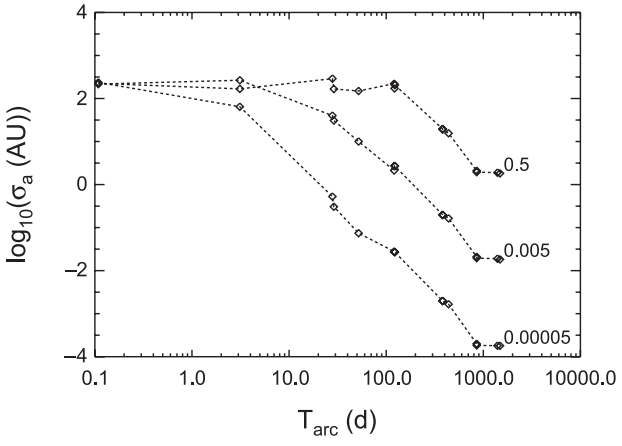


**Fig. 5.** Time evolution of semimajor-axis uncertainty for improving observational accuracy of a simulated dataset. More precise astrometric data can shorten the time required to reach the phase transition. In the case of (87269), the present orbital accuracy would have been reached in ~3 months with the expected accuracy of Pan-STARRS and in ~10 d with Gaia accuracy.

In order to check the orbital stability, one may integrate the orbits for a few millions of years and check for possible encounters. For the MC sampled orbital-element p.d.f.s, this would be an extremely time-consuming procedure. We therefore implement a stability criterion based just on the computed orbital elements. The filtering process is described in detail in *Virtanen et al.* (2003); we hereby present a summary of it. We perform an analysis of the minimum orbital intersection distances (MOIDs) of all the orbits with respect to the four giant planets, namely Jupiter, Saturn, Uranus, and Neptune. We have defined a possible close planetary approach as MOID being less than 3 Hill radii ($r_H$) from the planet. A low MOID would generally imply a close approach to the planet, unless the object is protected by a mean-motion resonance with the corresponding planet. We only check for mean-motion resonance with Neptune, because a capture into a resonance by the other giant planets in the Centaur region would generally be short-term in nature. To confirm a resonance capture, the orbit needs again to be numerically integrated for several million years to check whether the resonance argument of the expected resonance is librating or circulating (as done in G07). Instead, to obtain a preliminary estimate, we have adopted a simpler criterion based on proximity to the theoretical location of the libration zone. If in the a–e plane the orbit falls inside any region of possible libration with respect to Neptune, the orbit is tentatively considered to be in the resonance. The libration zones are taken from Fig. 1 of *Morbidelli et al.* (1995) up to the 1:6 resonance, assuming a diamond shape in the a–e plane and a maximum width of 2 AU. Since we have seen that there are objects in higher-order resonances, we extend their figure to include resonances from 1:7 to 1:21 using the above parameters for the libration zones. For multiapparition objects, the fraction of nonresonant objects with low MOIDs is just 4%. For one-apparition objects, 99% have at least one orbit fulfilling these criteria, corresponding to 50% of the total number of orbits. We thus conclude that the huge orbital uncertainties present for the one-apparition objects actually imply a large variety of possible dynamical evolutions for the objects, not all of which are realistic considering our current understanding of the dynamics of the outer solar system.

For some of the objects, more than 95% of the computed orbits are nonresonant and have low MOIDs. These are objects that are very likely experiencing close encounters with the giant planets. A detailed analysis of these cases is out of scope for this chapter. Nevertheless, we would like to mention two examples with low MOID with respect to Neptune: a one-apparition object 2002 $PQ_{152}$ (Ranging

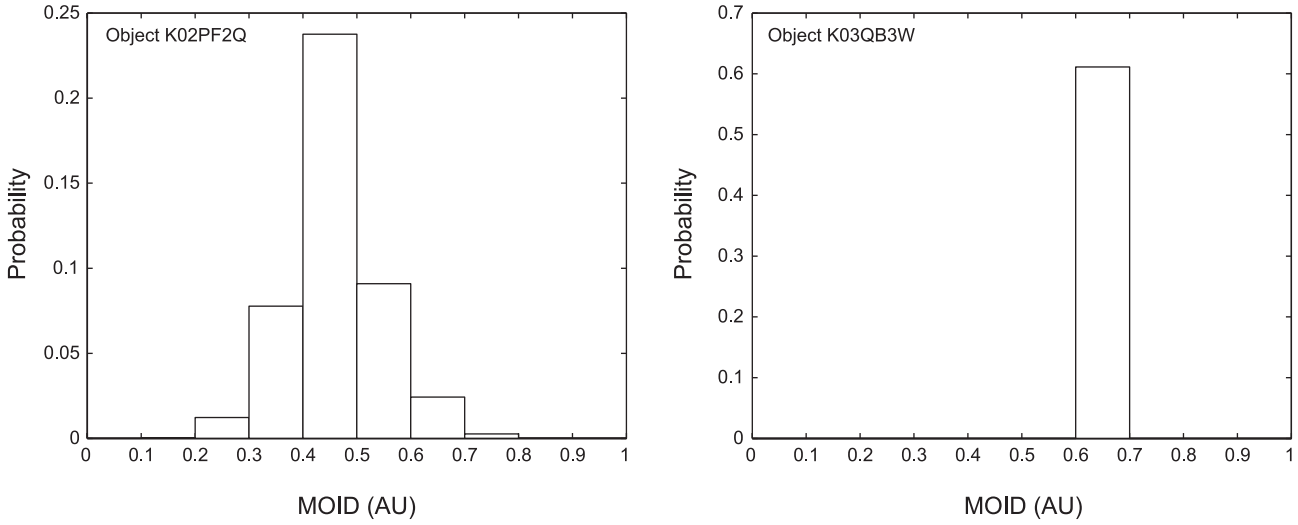


**Fig. 6.** Distribution of MOID values with respect to Neptune for two example cases, 2002 $PQ_{152}$ and 2003 $QW_{113}$.

solutions) and a two-apparition object 2003 $QW_{113}$ (VoV solutions). In Fig. 6 we present their MOID p.d.f.s with respect to Neptune. Note the spread in the MOID values for 2002 $PQ_{152}$ around a mean value of ~0.45 AU. Nevertheless, there are no solutions at very short distances that could imply a possible collision with the planet. The distribution of MOID values for 2003 $QW_{113}$ is well defined around a value of 0.65 AU.

The chances of a collision with Neptune among all the orbit solutions can be estimated to be very low but nonzero. We found 346 orbits among the total of approximately 1 million solutions for one- and two-apparition objects having MOIDs with respect to Neptune less than 3 planetary radius. A procedure to estimate the collision probability to any of the planets of a newly discovered object would be worth implementing.

### 3.3. Orbital Database

The current computations form the basis for a TNO orbital-element database. The orbital-element p.d.f.s are summarized in one of the following four formats: (1) ML orbital elements and standard deviations (e.g., least-squares solution), (2) a set of — all or best-fitting — sample orbits (e.g., from Ranging), (3) a set of orbital elements mapping the boundaries of the uncertainty region (from the VoV technique). In addition, orbit solutions after the filtering procedure can be obtained. The database is available from the authors (contact J. Virtanen).

The second and third format can be useful in more detailed dynamical studies, where a set of sample orbits mapping the orbital uncertainty can be used as initial values for numerical integrations. This kind of approach has been used for analyzing resonance occupation (*Chiang et al.,* 2003; *Elliot et al.,* 2005; see also G07). Another application of the database is in ephemeris prediction. The difficulty there is that the mapping of the uncertainty region from orbital-element space to sky-plane coordinates is nonlinear. While in the linear approximation, LSL covariance can be directly transformed into the sky-plane coordinates (see equation (7)), in the nonlinear case the full orbital-element p.d.f. needs to be propagated. Another solution for this nonlinear mapping problem has been given by *Milani* (1999) in terms of semilinear confidence boundaries and it has been widely used for asteroid recovery. The AstDys database offers orbital elements and covariances also for TNOs, but does not currently provide information on the nonlinearities that are dominant for the majority of objects in this short-arc population.

## 4. PREDICTION PROBLEMS

### 4.1. Ephemeris Uncertainty

Because of the nearly linear motion of TNOs, the projection of the element p.d.f. to the sky plane typically results in fairly linear distribution even if the original p.d.f. is highly nonlinear. This behavior is in contrast to the near-Earth objects (NEOs), for which the sky-plane uncertainties based on short-arc orbits quickly extend all over the celestial sphere. While the NEO community includes a large group of follow-up astrometrists, this is not the case for TNOs. Most of this is due to the large size of the telescope required for routine followup, as well as the long integration times required, which makes the efficiency of TNO observing rather low ("time spent per object" is high).

The BK method was designed for the practical purpose of helping observers to evaluate sky-plane uncertainties for the costly observations of TNOs. It has turned out as a useful tool for followup in several surveys; the method has been applied to objects discovered in the Deep Ecliptic Survey (*Millis et al.,* 2002; *Elliot et al.,* 2005) as well as in the Very Wide component of the Canada-France-Hawaii Telescope Legacy Survey (*Jones et al.,* 2006).

To illustrate the current ephemeris uncertainty for the population, the orbital-element p.d.f.s described in section 3

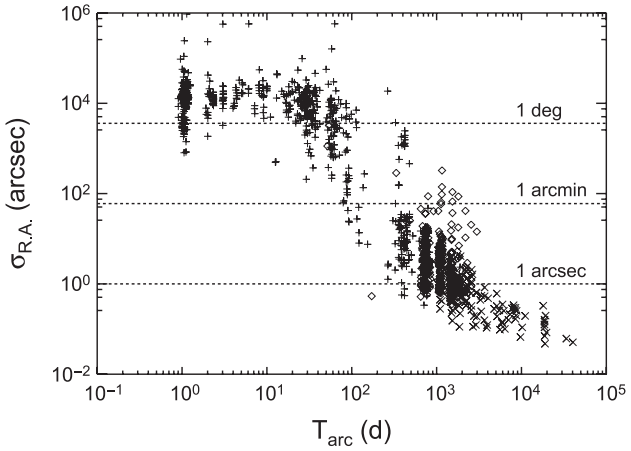


**Fig. 7.** Current ephemeris uncertainties for the known TNOs in terms of the standard deviation of the R.A. marginal p.d.f.s (July 4, 2006). A large majority of the one-apparition objects can be considered lost, and for several numbered objects (stars) the current uncertainty in their position is already close to 10 arcsec. Symbols as in Fig. 1.

have been propagated to a joint epoch and transformed into spherical coordinates. Figure 7 illustrates ephemeris uncertainty with the help of the standard deviations of the R.A. marginal p.d.f.s. The relevance of recovery attempts depends on the size of the sky-plane uncertainty region to be searched. Assuming that, in practice, 1σ uncertainty in R.A. (or Dec.) over 1° means that an object is lost, nearly half of the known population is beyond routine recovery.

At discovery, the MPC usually attempts to place each object in one of a few narrow dynamical classes, such as "plutino," "cubewano," or "scattered-disk object." While this may aid recovery of the object in the future if the guess is correct, it can also result in the loss of an object. Because of the large uncertainties involved for short-arc objects, reclassifications of TNOs in MPC listings are frequent (listed in the web-based *Distant EKOs Newsletter*). The probabilistic approach to orbit computation makes dedicated recovery attempts possible, however. With the help of Bayesian *a priori* information, wide ephemeris uncertainties can be constrained and an observing strategy can be planned (*Virtanen et al.,* 2001). As *a priori* knowledge, one can use dynamical filtering based on the TNO classification scheme (see section 4.2) or a full *a priori* p.d.f. based on, preferably unbiased, orbital-element distribution of known TNOs.

In an ideal search program, the followup of discovered objects is carried out as part of the survey. While the observing concept of future all-sky surveys will ensure followup more or less automatically, this has not been the case with past and current surveys. The natural goal of astrometric followup is to secure TNO orbits, as a result of which they are eventually assigned a number. As with asteroids, the condition for numbering is that the orbital uncertainties are considered small enough to enable routine followup observations for a reasonable time into the future. The ephemeris uncertainties for the known objects were propagated 10 years ahead from the last observation for each object. For the numbered objects, the 1σ uncertainties are mostly in the arcsecond level but, for several cases, the uncertainty grows to tens of arcseconds, or even arcminutes, if followup observations were to cease for 10 years. This highlights the need for continuous astrometric efforts for these distant objects.

While the question of optimized observing strategy may become to a large degree obsolete in the next few years, it will still be important for so-called science alerts, which are typically new discoveries with some property that makes them require immediate attention. Depending on the observing concept of the survey in question, there may be need for external observing efforts before the routine recovery by the survey itself.

### 4.2. Dynamical Classification

One of the first questions one wants to pose once a discovery of a new solar system object has been made is whether this object can be classified in one of the known dynamical groupings. While finding the answer to this question might not be as crucial and urgent for TNOs as it is for Earth-approaching objects, it is nevertheless needed in order to form a dynamical picture of our planetary system. Statistical methods provide firsthand tools for dynamical classification.

The final classification algorithm requires detailed dynamical studies using numerical integrations, and for the multiapparition objects, that has been the subject of G07, where the BK method is applied. Here we want to address the question of short-arc classification, and since this is by no means a static problem, we study the evolution of the classifications with the increasing observed time arc.

There has not been a clear consensus among the planetary research community about dynamical classification of the variety of solar system objects. In particular, the classification of TNOs has been the subject of many proposals, e.g., *Gladman et al.* (1998), G07, and *Virtanen et al.* (2003). Although we do not entirely agree with the classification scheme proposed by G07, we have adopted their scheme for consistency but introduced some modifications to speed up the short-arc classification process. As in section 3.2, to avoid heavy numerical integrations, we use some simpler criteria based on the orbital elements. We follow the flowchart of G07 presented in their Fig. 1 (left), but the resonance occupation is decided with a plot of the location of libration zones in the a–e plane, as explained in section 3.2. The other criteria based on the numerical integrations in G07's scheme is the classification of a scattered disk object (SDO). An SDO is by definition an object that has experienced close approaches to Neptune, and therefore the orbit must come close to that of the planet. We have adopted the criterion that SDOs should have a perihelion distance less than the semimajor axis of Neptune plus 3 $r_H$ of the planet (i.e., 2.3 AU), although it is not necessary that the MOID with respect to Neptune is that low at present. As we shall see, a large fraction of the short-arc orbits are retro-

grade. Retrograde orbits would have a Tisserand parameter with respect to Jupiter less than 3, and in many cases a negative value. In G07's scheme a retrograde orbit with small q would be incorrectly classified as a Jupiter-family comet. Therefore, we introduce a new criterion in the flow chart: In the second box from top to bottom, we ask if the orbit is retrograde (inclination greater than 90°).

We then have the following groups: (1) not the subject of this book (NotInc), (2) retrograde (Retro), (3) resonance (Res), (4) Jupiter-family comets (JFC), (5) Centaurs (Centa), (6) Inner Oort (InOort), (7) scattered disk objects (Scatt), (8) detached (Detac), (9) outer belt (Outer), and (10) classical belt (Class).

Using the orbital-element p.d.f.s computed either with Ranging, VoV, or least-squares estimation (section 3), we apply the classification scheme to the TNO population. Figures 8–10 show the phase-space structure of the transneptunian region. For one-apparition objects, the oversup-

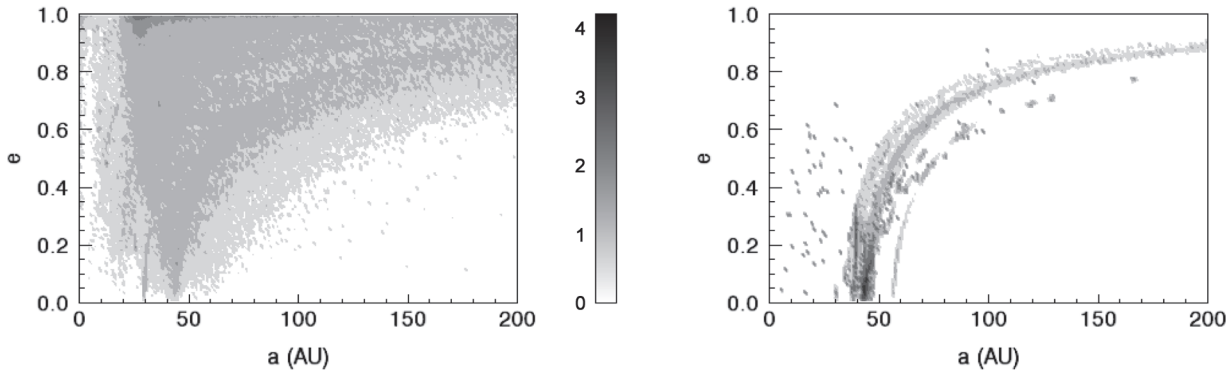


**Fig. 8.** Contour plot in the a–e plane illustrating the phase-space structure of the transneptunian region, left for $T_{arc} < 180$ and right for $T_{arc} > 180$ d. The intensity of the grayscale shading is proportional to $\sqrt{(N)}$, where N is the average number of objects in each bin (bin size 1 AU × 1 AU). The distribution is very flat for short-arc objects, illustrating the difficulty in their classification.

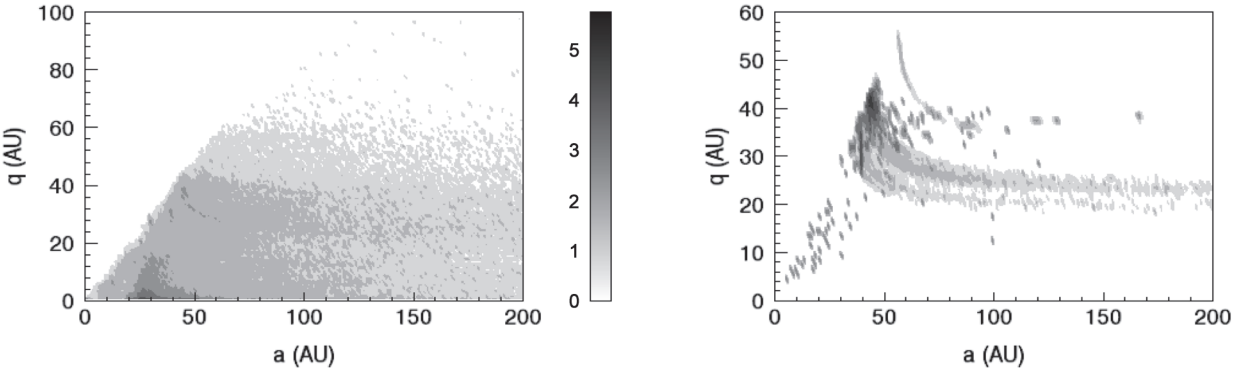


**Fig. 9.** As in Fig. 8 but in the a–q plane (bin size 1 AU × 1 AU).

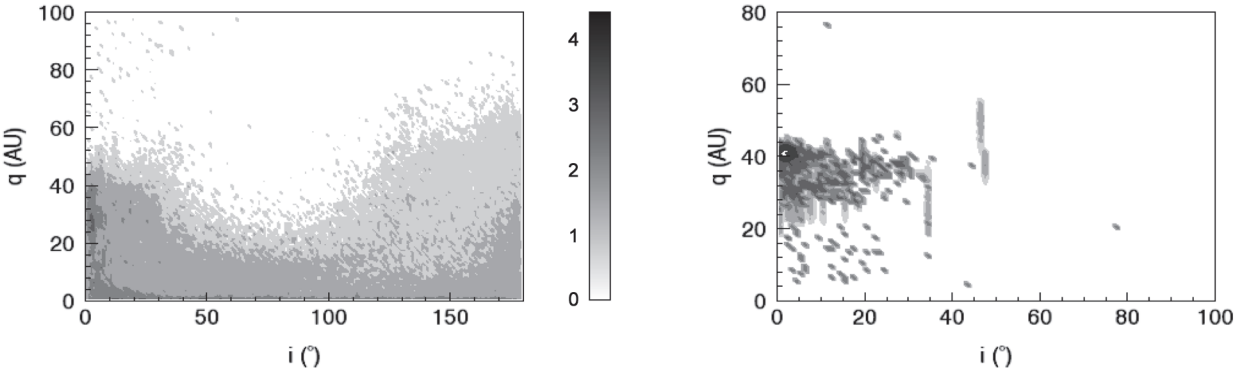


**Fig. 10.** As in Fig. 8 but in the i–q plane (bin size 1° × 1 AU). Note that the few vertically elongated clouds in the right plot correspond to objects with rather well-defined i but large uncertainties in q (i.e., in a and e).

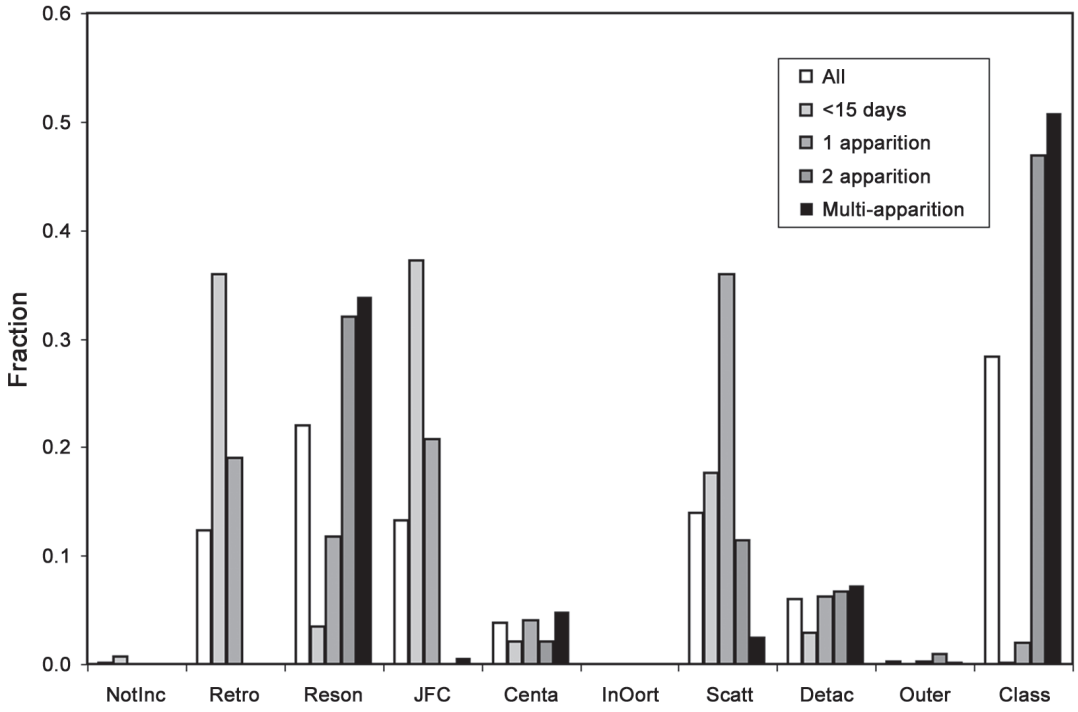


**Fig. 11.** Dynamical classification and its evolution as a function of increasing observational arc. The definitions for the different groupings are described in the text.

ply of high-eccentricity small-perihelion-distance orbits is again evident. The detailed dynamical structure of the region becomes visible, when only objects having observational arc $T_{arc} > 180$ d are included. The difficulty in the classification of objects becomes apparent from Fig. 11, which shows the probabilities for the adopted dynamical groupings for increasing observed time arcs. Short-arc data is well represented with cometary-type and even retrograde orbits. Thus even the TNO membership of these very-short-arc objects is uncertain. The percentages of two- and multi-apparition objects are very similar in all the groups. Therefore, for a secure dynamical classification we require an observed arc longer than ~2 yr.

We would like to point out some potentially interesting cases. There has been discussion about the existence of the outer edge for the belt. Based on our classification, there are two confirmed objects, which are outside the 2:1 resonance and in low-e orbits. 2003 $UY_{291}$ is very close to the classical population with $(a, e, i)_{ML} = (49.7, 0.18, 3.5)$, while 2004 $XR_{190}$ is clearly on the outside: $(a, e, i)_{ML} = (57.4, 0.11, 46.7)$ (see also *Allen et al.,* 2006). From Fig. 8 for the one-apparition objects, there is evidence for new candidates for the Neptune Trojans, and in fact, during the writing of this chapter, second-apparition data became available for two objects (2005 $TN_{53}$ and 2005 $TO_{74}$), which strengthen their Trojan classification. The existence of other short-arc Trojans needs to be studied with integrations.

A small fraction of objects exist that could not be classified in any of the proposed groupings. There are in particular two short-arc objects [2004 $PR_{107}$ (two observations, one day) and 2001 $DU_{108}$ (four observations, three days)] that have a high probability of being inner-solar-system objects. With their current datasets, their classification is extremely uncertain and NEO classification cannot be overruled.

## 5. CONCLUSION

We have reviewed the orbit computation problem in the transneptunian region. While the TNO population continues to be a poorly observed one after over a decade of dedicated observations, the recent advances in orbit computation methods help us to examine the TNO orbital uncertainties even from exiguous data. Careful assessment of orbital uncertainties of the population is in place for several reasons. First of all, to keep track of the discovered objects, their sky-plane uncertainties need to be estimated. The orbital information is the starting point for the attempts to define the dynamical structure of the transneptunian region as well as for deriving unbiased orbital distributions. Also, the correlation between TNO physical and dynamical properties are of interest. These are topics that are discussed in other chapters of this volume.

We have described the numerical methods available for TNO orbit computation. Nearly half the population have been observed during one apparition only, and thus their large uncertainties need to be estimated with a fully nonlinear inversion method. Ranging efficiently unveils the extended orbital-element p.d.f.s and strongly nonlinear cor-

relations between elements. BK and VoV methods have been developed and shown to successfully handle cases of more modest orbital uncertainties. While the Monte Carlo methods are today feasible to use due to computer resources available, methods using linearization are attractive due to their speed whenever the approximation can be justifiably adopted. In particular, linearized methods suffice in most cases for ephemeris prediction due to the nearly linear TNO motions.

An important application for the orbital information is in classification of the discovered objects. Due to the large uncertainties involved, dynamical classification based on one-apparition data is highly uncertain. Any detailed dynamical analysis of the population should be based on multiapparition data. In the statistical approach for orbit computation, tentative classification can still be made by assigning an object probabilities for being in the different groupings. Such information can be used, for example, as constraining *a priori* information in recovery attempts.

We note that the dynamical model adopted in TNO orbit computation should be studied further. Previously, it has been general practice to consider perturbative forces of the nine planets in orbit integrations, but recently our view of the solar system has been revisited. It would be interesting to study in practice what the effect of (134340) Pluto is in TNO orbit computation. In a similar manner, the perturbative effects of the other large objects, such as (136199) Eris, as well as the effect of mutual close encounters between TNOs on orbit computation will be a subject for further studies.

Should studies of TNO collisions within timescales of tens of thousands of years be of interest, the orbital-element p.d.f.s allow detailed monitoring and evaluation of mutual close approaches among TNOs as well as TNO close approaches to giant planets. It is evident from the p.d.f.s of TNOs with exiguous observational data that, within the orbital uncertainties, a wide spectrum of dynamical evolutions be possible for individual TNOs. Furthermore, TNO orbital-element p.d.f.s can mimic cometary orbital-element p.d.f.s and thereby offer test cases for the assessment of terrestrial collision probabilities for long-period comets. The advent of next-generation astrometric surveys will have a large impact on TNO orbits but they will also introduce new challenges for orbit computation. Deep all-sky observations will accumulate huge databases of observations for solar system objects, which need to be correctly linked and identified with known objects (e.g., *Granvik and Muinonen,* 2005; *Milani et al.,* 2005). For TNOs, Ranging has already been used to automatically verify linkages between observation sets from different apparitions (*Virtanen et al.,* 2003), and the approach by *Granvik and Muinonen* (2005) is straightforward to implement for the search of linkages between short-arc observation sets of TNOs. On the other hand, improving astrometric accuracies will unveil the coupling of physical and dynamical properties of the objects and make it necessary to solve for them simultaneously. With much of the work already underway, we can in a decade anticipate having an improved TNO orbit database with an increase by a factor of several in the number of objects included, with a similar improvement in their estimated orbital accuracies.

***Acknowledgments.*** We thank the two reviewers for constructive comments. J.V. wishes to thank M. Granvik for software development for the Orb package as well as helpful discussions on orbits in general. The research of J.V. was, in part, supported by the Magnus Ehrnrooth Foundation.

## REFERENCES

Allen R. L., Gladman B., Kavelaars J., Petit J-M., Parker J., and Nicholson P. (2006) Discovery of a low-eccentricity, high inclination Kuiper belt object at 58 AU. *Astron. J., 640,* 83–86.

Bernstein G. M. and Khushalani B. (2000) Orbit fitting and uncertainties for Kuiper belt objects. *Astron. J., 120,* 3323–3332.

Bowell E., Virtanen J., Muinonen K., and Boattini A. (2002) Asteroid orbit computation. In *Asteroids III* (W. F. Bottke Jr. et al., eds.), pp. 27–43. Univ. of Arizona, Tucson.

Box G. E. P. and Tiao G. C. (1973) *Bayesian Inference in Statistical Analysis.* Addison-Wesley, Reading, Massachusetts.

Carpino M., Milani A., and Chesley S. R. (2003) Error statistics of asteroid optical astrometric observations. *Icarus, 166(2),* 248–270.

Chesley S. R. (2005) Very short arc orbit determination: The case of 2004 $FU_{162}$. In *Dynamics of Populations of Planetary Systems* (Z. Knežević and A. Milani, eds.), pp. 255–258. Cambridge Univ., Cambridge.

Chiang E. I. and 10 colleagues (2003) Resonance occupation in the Kuiper Belt: Case examples of the 5:2 and Trojan resonances. *Astron. J., 126,* 430–443.

Chodas, P. W. and Yeomans D. K. (1996) The orbital motion and impact circumstances of comet Shoemaker-Levy 9. In *The Collision of Comet Shoemaker-Levy 9 and Jupiter* (K. S. Noll et al., eds.), pp. 1–30. Cambridge Univ., Cambridge.

Elliot J. L., Kern S. D., Clancy K. B., Gulbis A. A. S., Millis R. L., et al. (2005) The Deep Ecliptic Survey: A search for Kuiper belt objects and Centaurs. II. Dynamical classification, the Kuiper belt plane, and the core population. *Astron. J., 129,* 1117–1162.

Gladman B., Kavelaars J. J., Nicholson P. D., Loredo T. J., and Burns J. A. (1998) Pencil-beam surveys for faint trans-neptunian objects. *Astron. J., 116,* 2042–2054.

Goldader J. D. and Alcock C. (2003) Constraining recovery observations for trans-neptunian objects with poorly known orbits. *Publ. Astron. Soc. Pac., 115,* 1330–1339.

Granvik M. and Muinonen K. (2005) Asteroid identification at discovery. *Icarus, 179,* 109–127.

Granvik M., Virtanen J., Muinonen K., Bowell E., Koehn B., and Tancredi G. (2003) Transneptunian object ephemeris service (TNOEPH). In *First Decadal Review of the Edgeworth-Kuiper Belt* (J. K. Davies and L. H. Barrera, eds.), pp. 73–78. Kluwer, Dordrecht [reprinted from *Earth Moon Planets, 92(1–4)*].

Hestroffer D., Vachier F., and Balat B. (2005) Orbit determination of binary asteroids. *Earth Moon Planets, 97,* 245–260.

Jedicke R., Magnier E. A., Kaiser N., and Chambers K. C. (2007) The next decade of solar system discovery with Pan-STARRS. In *Near Earth Objects, Our Celestial Neighbors: Opportunity and Risk* (A. Milani et al., eds.), pp. 341–352. IAU Symposium No. 236, Cambridge Univ., Cambridge.

Jeffreys H. (1946) An invariant form for the prior probability in estimation problems. *Proc. R. Statistical Soc. London, A186,* 453–461.

Jones R. L., Gladman B., Petit J.-M., Rousselot P., Mousis O., et al. (2006) The CFEPS Kuiper belt survey: Strategy and presurvey results. *Icarus, 185,* 508–522.

Kaasalainen M., Hestroffer D., and Tanga P. (2005) Physical models and refined orbits for asteroids from Gaia photo- and astrometry. In *The Three Dimensional Universe with Gaia*, p. 301. ESA SP 576, European Space Agency, Noordwijk.

Kristensen L. K. (2004) Initial orbit determination for distant objects. *Astron. J., 127,* 2424–2435.

Lehtinen M. S. (1988) On statistical inversion theory. In *Theory and Applications of Inverse Problems* (H. Haario, ed.), pp. 46–57. Pitman Research Notes in Mathematical Series 167.

Menke W. (1989) *Geophysical Data Analysis: Discrete Inverse Theory*. Academic, New York.

Milani A. (1999) The asteroid identification problem I: Recovery of lost asteroids. *Icarus, 137,* 269–292.

Milani A. and Knežević Z. (2005) From astrometry to celestial mechanics: Orbit determination with very short arcs. *Celest. Mech. Dyn. Astron., 92,* 1–18.

Milani A. and Valsecchi G. B. (1999) The asteroid identification problem II: Target plane confidence boundaries. *Icarus, 140,* 408–423.

Milani A., Chesley S. R., Chodas P. W., and Valsecchi G. B. (2002) Asteroid close approaches: Analysis and potential impact detection. In *Asteroids III* (W. F. Bottke Jr. et al., eds.), pp. 55–70. Univ. of Arizona, Tucson.

Milani A., Gronchi G. F., Michieli Vitturi M., and Knežević Z. (2004) Orbit determination with very short arcs. I Admissible regions. *Celest. Mech. Dyn. Astron., 90,* 57–85.

Milani A., Gronchi G. F., Knežević Z., Sansaturio M. E., and Arratia O. (2005) Orbit determination with very short arcs. II Identifications. *Icarus, 179,* 350–374.

Milani A., Gronchi G. F., Knežević Z., Sansaturio M. E., Arratia O., Denneau L., Grav T., Heasley J., Jedicke R., and Kubica J. (2006) Unbiased orbit determination for the next generation asteroid/comet surveys. In *Asteroids Comets Meteors 2005* (D. Lazzaro et al., eds.), pp. 367–380. Cambridge Univ., Cambridge.

Millis R. L., Buie M. W., Wasserman L. H., Elliot J. L., Kern S. D., and Wagner R. M. (2002) The Deep Ecliptic Survey: A search for Kuiper belt objects and Centaurs. I. Description of methods and initial results. *Astron. J., 123,* 2083–2109.

Morbidelli A., Thomas F., and Moons M. (1995) The resonant structure of the Kuiper belt and the dynamics of the first five trans-Neptunian objects. *Icarus, 118,* 322–340.

Mosegaard K. and Tarantola A. (2002) Probabilistic approach to inverse problems. In *International Handbook of Earthquake and Engineering Seismology (Part A)* (W. H. K. Lee et al., eds.), pp. 237–265. Academic, New York.

Muinonen K. and Bowell E. (1993) Asteroid orbit determination using Bayesian probabilities. *Icarus, 104,* 255–279.

Muinonen K. and Virtanen J. (2002) Computation of orbits for near-Earth objects from high-precision astrometry. In *Proc. of the International Workshop on Collaboration and Coordination Among NEO Observers and Orbit Computers* (Kurashiki, October 23–26, 2001, Organized by Japan Spaceguard Association), pp. 105–113.

Muinonen K., Virtanen J., and Bowell E. (2001) Collision probability for Earth-crossing asteroids using orbital ranging. *Celest. Mech. Dyn. Astron., 81,* 93–101.

Muinonen K., Virtanen J., Granvik M., and Laakso T. (2006) Asteroid orbits using phase-space volumes of variation. *Mon. Not. R. Astron. Soc., 368,* 809–818.

Virtanen J. and Muinonen K. (2006) Time evolution of orbital uncertainties for the impactor candidate 2004 $AS_1$. *Icarus, 184,* 289–301.

Virtanen J., Muinonen K., and Bowell E. (2001) Statistical ranging of asteroid orbits. *Icarus, 154,* 412–431.

Virtanen J., Muinonen K., Tancredi G., and Bowell E. (2003) Orbit computation for transneptunian objects. *Icarus, 161,* 419–430.

Zacharias N. (2004) Astrometric reference stars: From UCAC to URAC. *Astron. Nachr. 325(6),* 631–635.